



Article

Biomorphic Fibrous TiO₂ Photocatalyst Obtained by Hydrothermal Impregnation of Short Flax Fibers with Titanium Polyhydroxocomplexes

Mikhail F. Butman ¹, Nataliya E. Kochkina ², Nikolay L. Ovchinnikov ¹, Nikolay V. Zinenko ¹, Dmitry N. Sergeev ³,* and Michael Müller ³

- Ivanovo State University of Chemistry and Technology, Sheremetevsky Avenue 7, 153000 Ivanovo, Russia; butman@isuct.ru (M.F.B.); ovchinnikovnl_1972@mail.ru (N.L.O.); nick653@mail.ru (N.V.Z.)
- G.A. Krestov Institute of Solution Chemistry, Russian Academy of Sciences, Akademicheskaya St. 1, 153045 Ivanovo, Russia; kochkinane@mail.ru
- Forschungszentrum Jülich GmbH, IEK-2, Leo-Brandt-Str.1, 52425 Jülich, Germany; mic.mueller@fz-juelich.de
- * Correspondence: d.sergeev@fz-juelich.de; Tel.: +49-2461-61-3280

Received: 24 April 2020; Accepted: 11 May 2020; Published: 13 May 2020



Abstract: A biomimetic solution technology for producing a photocatalytic material in the form of biomorphic titanium oxide fibers with a hierarchical structure using short flax fiber as a biotemplate is proposed. The impregnation of flax fibers intensified under hydrothermal conditions with a precursor was performed in an autoclave to activate the nucleation of the photoactive TiO₂ phases. The interaction between precursor and flax fibers was studied by using infrared spectroscopy (IR) and differential scanning calorimetry/thermogravimetry analysis (DSC/TG). The morphology, structure, and textural properties of the TiO₂ fibers obtained at annealing temperatures of 500–700 °C were determined by X-ray diffraction analysis, scanning electron microscopy, and nitrogen adsorption/desorption. It is shown that the annealing temperature of the impregnated biotemplates significantly affects the phase composition, crystallite size, and porous structure of TiO₂ fiber samples. The photocatalytic activity of the obtained fibrous TiO₂ materials was evaluated by using the decomposition of the cationic dye Rhodamine B in an aqueous solution (concentration 12 mg/L) under the influence of ultraviolet radiation (UV). The maximum photodegradation efficiency of the Rhodamine B was observed for TiO₂ fibers annealed at 600 °C and containing 40% anatase and 60% rutile. This sample ensured 100% degradation of the dye in 20 min, and this amount significantly exceeds the photocatalytic activity of the commercial Degussa P25 photocatalyst and TiO2 samples obtained previously under hydrothermal conditions by the sol-gel method.

Keywords: hierarchical structure; biomorphic fibers TiO₂; Titanium polyhydroxocomplexes; adsorption; photocatalytic activity

1. Introduction

Among various photoactive materials, TiO_2 is recognized to be one of the most effective semiconductor photocatalysts for the decomposition or oxidation of organic pollutants in a liquid medium. Moreover, its high photocatalytic activity combines with chemical inertness, non-toxicity, low cost, and environmental friendliness [1–3]. It is known that the photocatalytic activity of TiO_2 depends on the phase composition, crystallinity, and specific surface area that are determined, as a rule, by the photocatalyst preparation method [4–6].

To increase the photocatalytic activity of titanium oxide by enhancing the light absorption, as well as diffusion and adsorption of reagent molecules, an approach related to the production of TiO₂ in the form of a material with a hierarchical morphological structure was proposed [7–9].

Catalysts 2020, 10, 541 2 of 14

It contains structural elements with sizes in a wide range of values from nano- to several tens of micrometers, including micro-, meso-, and macropores [10,11]. The presence of interconnected pores with various sizes in the catalyst structure ensures high diffusion efficiency of the reagents subjected to photodegradation.

The biomimetic method is one of the most effective, simple and cheap methods for obtaining materials with hierarchical morphology. It is based on the application of natural templates, which are impregnated with a precursor, followed by drying and burning. Among the common biotemplates, one can distinguish various cellulosic materials (wood pulp, cotton, filter paper) having a multimeric arrangement with a system of pores and capillaries [12–18].

Almost all known biotemplate methods for TiO_2 production using cellulosic materials imply the formation of a TiO_2 sol layer on the fiber surface. In this case, the treatment of cellulose fibers is carried out with solutions of alcoholates and other titanium compounds, including sol-gel methods [12–16,19]. However, the methods for TiO_2 fibers production by applying a sol to cellulose have a number of disadvantages, such as: the high labor input, the complexity of the procedures, and the problem of destruction of hollow fibers during their preparation [20].

In our previous work, we have proposed [21] an appropriate approach to the preparation of biomorphic TiO₂ with a hierarchical structure based on the impregnation of the biotemplate—wood pulp—with a solution of large-sized hydrolytic forms of titanium, which are formed at the intermediate stage of the transition of the solution to sol and are effectively being sorbed by cellulose fiber. It should be noted that in practice solutions of titanium hydroxocomplexes were previously used only for the preparation of pillared clays, which are effective catalysts and sorbents [22-24]. In our previous study [25], the production of TiO₂-pillared montmorillonite using solutions of titanium hydroxocomplexes was described. It was found that application of hydrothermal treatment at the stage of pillaring allows for increasing the degree of crystallinity of TiO2 and thereby improves the photocatalytic properties of the obtained material. When using hydrothermal treatment in biotemplate synthesis, it is necessary to take into account the fact that the preparation of stable forms of titanium hydroxocomplexes requires high concentration of an acid [22]. Under these conditions, some biotemplates, for example wood pulp, can be decomposed. Therefore, it is necessary to choose a template with higher acid resistance. From this point of view, a short flaxen fibre is a suitable candidate, which is in fact a waste remaining after flaxen trusts machining and which is not further used in spinning to obtain flaxen fabrics. Flax fiber has a complex multimeric structure with a system of pores and capillaries and also includes elementary cellulose fibers—polymers consisting of β-D-glucopyranose units with hydroxyl groups. These fibers, as the main components of flax, are capable of sorbing from a solution polycations—precursors of the photocatalyst, as well as of accelerating the nucleation and growth of its particles under hydrothermal conditions.

In the present work, we aim to obtain fibrous TiO_2 with high photocatalytic activity by the biotemplate method by the use of impregnating a short flax fiber with a precursor solution. To activate the nucleation of photoactive precursor particles, the process was carried out in an autoclave. In this work, we considered the influence of the hydrothermal effects and the annealing temperature on the structure, texture properties, and photocatalytic activity of the obtained TiO_2 .

2. Results and Discussion

The particle size distribution of titanium hydroxocomplexes in a precursor solution is shown in Figure 1. It can be seen that the modal value of the size of the complexes is 1.5 nm. This size allows for supposing the uniformity of impregnation in comparison with sol precursors, and retains the possibility of efficient nucleation of nano- and microcrystallites in the body of the biotemplate.

Catalysts 2020, 10, 541 3 of 14

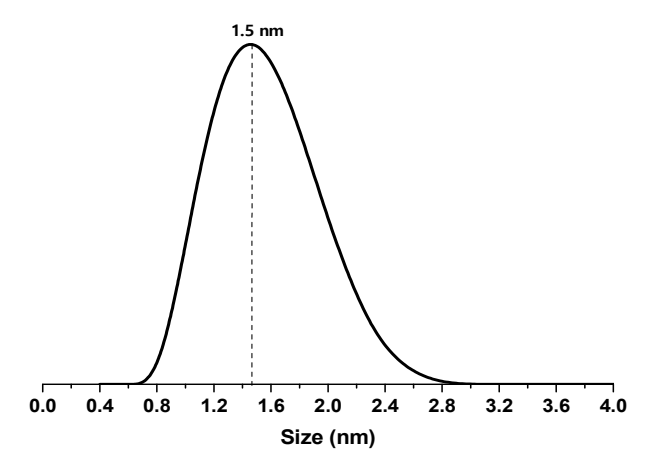


Figure 1. Hydrodynamic diameter distribution in the 0.56 M solution of titanium hydroxocomplexes.

To identify the patterns of formation of fibrous TiO₂ during the flax fibre impregnation process, IR spectra of the biotemplate were studied before and after impregnation with a solution of titanium hydroxocomplexes (0.56 M) using hydrothermal influences (Figure 2).

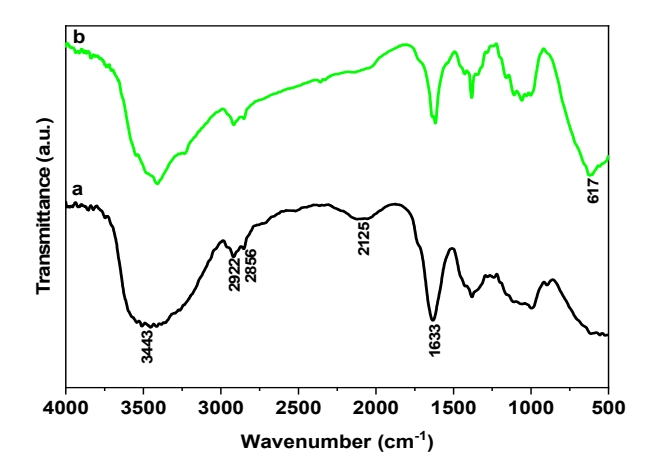


Figure 2. FTIR spectra of flax fiber before (a) and after (b) impregnation with a solution of titanium hydroxocomplexes.

As it can be seen from Figure 2, impregnation of flax fiber with a precursor solution leads to some changes in the IR spectrum. First of all, there is a narrowing and a slight decrease in the intensity of the absorption band in the region of 3000–3600 cm⁻¹ caused by stretching vibrations of OH bonds included in hydrogen bonds. In addition, the band intensity decreases noticeably at 2125 cm⁻¹, and it indicates the presence of nitrogenous substances in the biotemplate. A decrease in the intensity of the bands at 2922, 2856, and 1633 cm⁻¹ is observed, which is caused by deformation vibrations of the CH bond in the CH₂ and CH groups of hemicellulose [26,27]. The most probable cause of such changes in the spectrum of raw flax fiber is the destruction of impurities associated with cellulose as a result of their acid hydrolysis in a solution of titanium hydroxocomplexes. Hydrothermal conditions contribute to the intensification of the hydrolytic destruction of the components of the incrusts and the carbohydrate complex of flax fiber, as well as to its release from the decay products of impurities. An indirect confirmation of these effects is the intense brown coloring of the precursor solution after treating flax fibers in it, and such a color is typical for solutions of impurities of flax fibers.

In addition, an absorption band at 617 cm⁻¹ arises in the sample of the impregnated biotemplate, which corresponds to stretching vibrations of the Ti–O groups characteristic of titanium dioxide [28,29].

Catalysts 2020, 10, 541 4 of 14

This means that formation of TiO₂ in the biotemplate structure begins even at the stage of impregnation in an autoclave.

To study the burning process of the impregnated flaxen template, a TG/DSC analysis was used. Two samples before and after impregnation with a solution of titanium hydroxocomplexes were studied under air atmosphere. The results are shown in Figure 3.

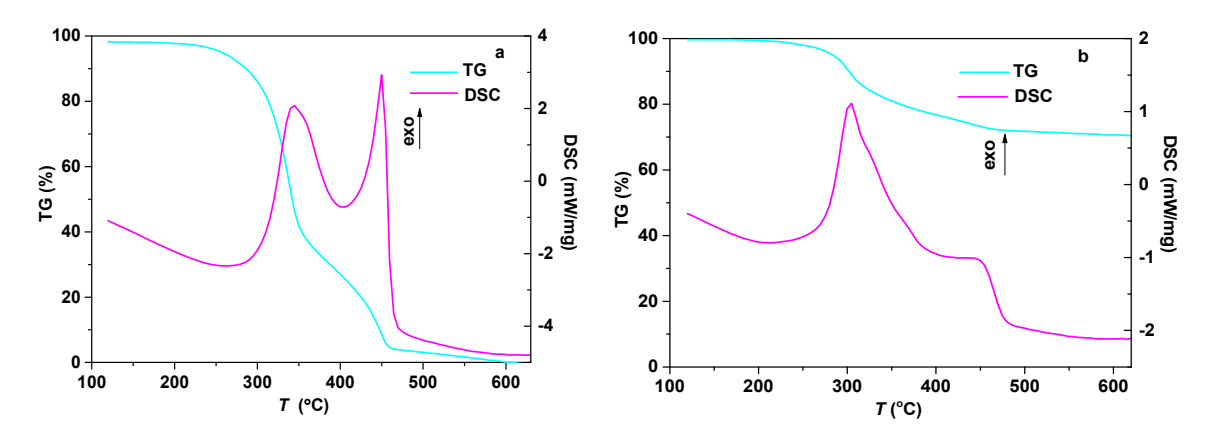


Figure 3. TG/DSC thermograms of the flax fiber before (**a**) and after (**b**) impregnation with a solution of titanium hydroxocomplexes.

In both cases, burning starts around 250 °C and finishes at 450 °C. This process is going in two stages, as it can be seen from DSC as well as from the TG signal. In the first case, the process ends with a complete burnout of the material under study. In the case of an impregnated sample, the processes of oxidation and thermal destruction occur simultaneously with the thermolysis of the precursor salt and the formation of titanium oxide. All these effects can be overlapped with each other and make it difficult to analyze the results in detail. The main difference between these two samples is the weight loss, which shows formation of TiO_2 fibers after impregnation (67%).

To determine the phase composition and sizes of the corresponding crystallites of titanium oxide samples, XRD analysis was performed. The results are presented in Figure 4 and Table 1.

The results demonstrate that an increase in the annealing temperature is naturally accompanied by the conversion of metastable anatase to stable rutile. At the same time, the temperature increase causes the growth of TiO_2 crystallites. The results of the texture properties of fibrous TiO_2 samples studied by the method of low-temperature adsorption/desorption of N_2 are presented in Figure 5 and in Table 2.

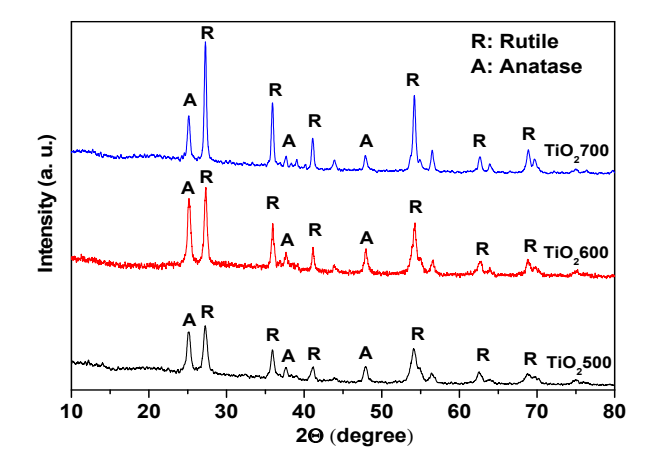
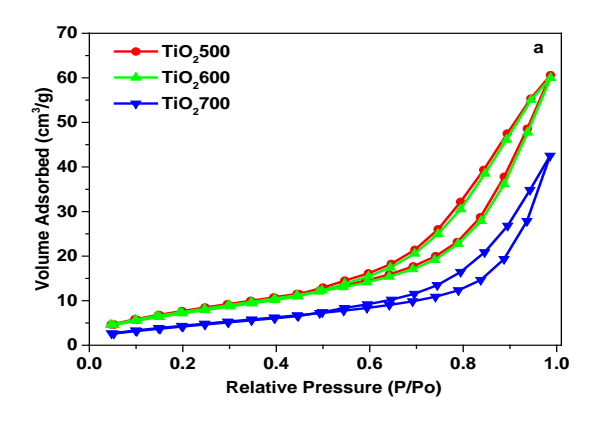


Figure 4. X-ray patterns of fibrous TiO_2 .

Catalysts 2020, 10, 541 5 of 14

Sample	Average Crystallite Sizes, nm		Phase Composition, %	
	A	R	A	R
TiO ₂ 500	15.7	19.2	50	50
TiO ₂ 600	21.6	27.7	40	60
TiO_2700	40.0	45.0	25	75

Table 1. Phase composition and average crystallite size of the fibrous TiO_2 .



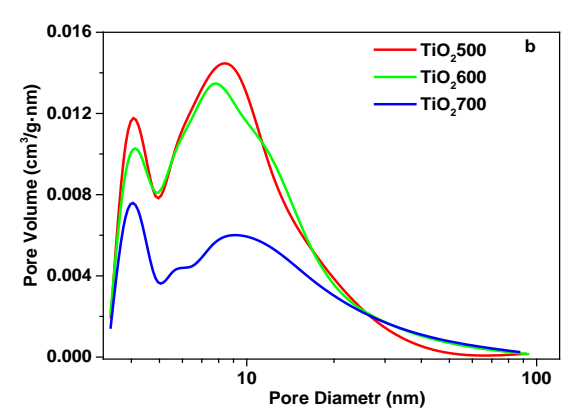


Figure 5. Nitrogen adsorption–desorption isotherms (a) and pore size distribution (b) of fibrous TiO_2 samples obtained at various annealing temperatures.

Table 2. Porosimetry data for the fibrous TiO₂ samples.

Sample	S _{BET} (Mesopores) (m ² /g)	V _{Total} (cm ³ /g)	V_{BJH} (cm ³ /g)	D _p (nm)
TiO ₂ 500	30.21	0.093979	0.0884885	7.70637
TiO ₂ 600	29.23	0.093046	0.0882438	7.69106
TiO ₂ 700	17.46	0.065963	0.0551854	7.28634

The nitrogen adsorption isotherms of the prepared samples belong to the type IV and have a hysteresis loop of type H3 (according to the IUPAC classification), typical for mesoporous materials [30]. Temperature variation of the annealing of the flaxen template in the range of 500–600 °C has a weak effect on the texture characteristics of TiO₂. At 700 °C, a significant decrease of the S_{BET} value is observed.

The morphology of the initial biotemplate and the obtained TiO_2 fibers was studied by SEM. Figure 6 presents the images of the hierarchical structural arrangement of the studied samples.

On the surface of the biotemplate residues, accompanying flaxen cellulose substances (hemicelluloses, pectin, and lignin) are visible. The cell wall of an elementary fiber consists of strongly oriented mesofibril cellulose, which is about 200 nm thick, embedded in a matrix consisting of hemicellulose and lignin [31]. In addition, pores up to 250 nm in size are visible in the flax fiber wall. A fibrous TiO₂ sample is a ceramic replica of a biotemplate having a corpuscular-spongy texture and hierarchical organization, which is characterized by the presence of crystallites agglomerated in the longitudinal direction with micro- and mesopores in between.

The size of TiO_2 crystallite agglomerates is relatively large (about 500–700 μ m), which also confirms the fact of TiO_2 formation at the beginning of the stage of impregnation of the biotemplate in the autoclave studied by IR spectroscopy. The continuation of annealing leads to further crystal growth and to agglomeration of titanium oxide fibers with crystallites sintered together.

Catalysts 2020, 10, 541 6 of 14

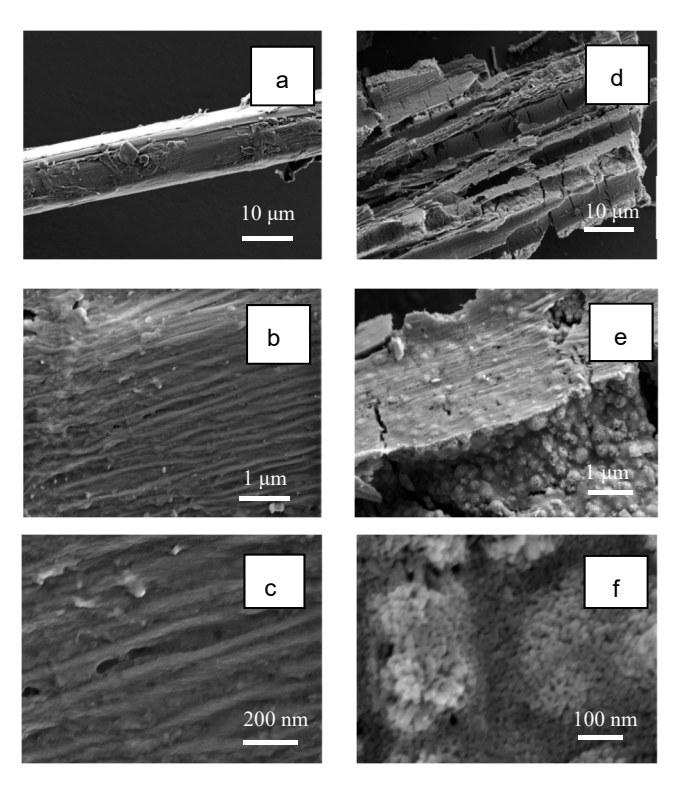


Figure 6. SEM images of the flax template (a-c) and fibrous TiO₂600 (d-f).

The photocatalytic activity of fibrous TiO_2 samples was evaluated according to the decomposition of the Rhodamine B dye as a model substance under the influence of ultraviolet radiation. This dye degradation mechanism [32–37] and its theoretical explanation [38] using different forms of TiO_2 photocatalysts were previously thoroughly studied. It allows us to compare the photocatalytic activity of our TiO_2 samples with the literature data. As it is already known, the efficiency of dye removal from aqueous solutions on a photocatalyst is determined by the additive adsorption and photocatalysis process. We studied the kinetics of Rhodamine B adsorption by the fibrous TiO_2 (Figure 7). The kinetic curves have similar shape. The difference can be seen only in the amount of adsorbed substance at equilibrium state, which was established in all cases within about 30 min.

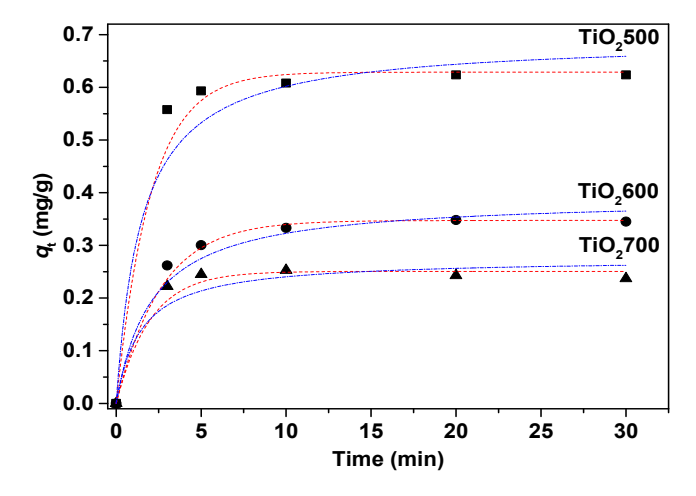


Figure 7. Kinetic adsorption curves of Rhodamine B dye at 20 °C on the obtained fibrous TiO₂ samples: red, Lagergren (pseudo-first order) model: blue, Ho and McKay (pseudo-second order).

Catalysts 2020, 10, 541 7 of 14

After a 30-min contact of the phases in the series of samples TiO_2700 , TiO_2600 , and TiO_2500 , the adsorption capacity with respect to Rhodamine B is successively increased. TiO_2500 removed 37% of the dye from the solution, while TiO_2600 and TiO_2700 removed 20% and 14%, respectively. The data on adsorption capacity correlate well with the texture properties of photocatalysts (Table 2).

To describe the kinetics of adsorption, we used the well-known kinetic models of pseudo-first order Lagergren [39] and pseudo-second order Ho and Mackay [40], which can be represented by Equations (1) and (2), respectively:

$$Q_t = Q_e(1 - \exp^{-k_1 t}), \tag{1}$$

$$Q_t = \frac{k_2 Q_e^2 t}{1 + k_2 Q_e t} \tag{2}$$

 $Q_{\rm t}$ and $Q_{\rm e}$ in mg/g are the quantity of adsorbed dye per unit mass of the sorbent at a given time t and at equilibrium, respectively; k_1 and k_2 are the adsorption rate constants of the pseudo-first (min⁻¹) and pseudo-second order (g mg⁻¹ min⁻¹), respectively. The criterion for the adequacy of kinetic models was the coefficient R^2 . The obtained parameters are given in Table 3.

Kinetic Model	TiO ₂ 500	TiO ₂ 600	TiO ₂ 700
Pseudo-first order			
$Q_{\rm e}~({\rm mg~g^{-1}})$	0.615	0.342	0.245
$k_1 (\text{min}^{-1})$	0.800	0.460	0.809
R^2	0.999	0.998	0.996
Pseudo-second order			
$Q_{\rm e}~({\rm mg~g^{-1}})$	0.626	0.365	0.248
$k_2 (g mg^{-1} min^{-1})$	5.549	2.450	16.440
R^2	0.996	0.999	0.992

Table 3. Parameters of Rhodamine B dye adsorption kinetics for the obtained fibrous TiO₂ samples.

The obtained values of R^2 indicate the applicability of pseudo-first and pseudo-second order kinetic models for describing the kinetics of Rhodamine B adsorption on fibrous TiO_2 . Considering higher R^2 values, preference should be given to a pseudo-first order kinetic model which indicates that sorption is preceded by diffusion. The obtained results show that the processes that control the kinetics of absorption of the Rhodamine B dye by TiO_2 fiber samples are most likely to be both physical and chemical sorption [41].

The results of the study of the UV photolysis of the Rhodamine B dye in an aqueous solution in the presence of the obtained photocatalyst samples (measurements were performed after 30 min of sorption) are presented in Figure 8. For comparison, the kinetic curve obtained using a commercial Degussa P-25 catalyst is also shown in this figure.

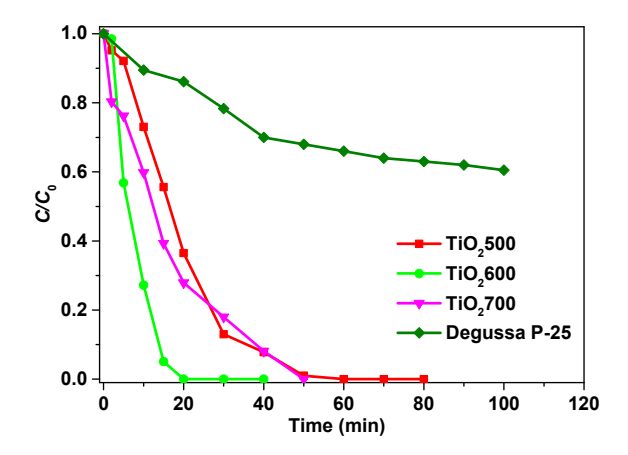


Figure 8. Photocatalytic degradation of RhB dye under UV irradiation.

Catalysts 2020, 10, 541 8 of 14

It can be seen that all studied samples of fibrous TiO₂ are characterized by improved photocatalytic activity in comparison with a commercial photocatalyst.

Among all fibrous TiO₂ samples synthesized in this work, the highest photocatalytic activity was observed for TiO₂600. Several factors are known to influence the activity of TiO₂ in the photocatalytic process, namely: texture properties that determine the sorption ability of the catalyst particles, crystallite size, and their phase composition [42]. All the TiO₂ samples obtained in this work were mixtures of anatase and rutile, which are known to be more effective in the photocatalytic process as the synergistic effect between the two phases reduces the recombination effect. For example, the authors of [43] experimentally observed that mixed-phase TiO₂ nanoparticles are significantly better photocatalysts than a simple mixture of single-phase nanoparticles due to their close-contact heterophase junctions, which are apparently also the case in the solution technology applied in this work. The conduction band electrons from the rutile phase are being transferred to the anatase phase due to favorable conduction band alignment, in this way inhibiting charge recombination [44,45]. Moreover, in a mixed anatase/rutile configuration, the lattices align to facilitate charge separation, thus enhancing the photocatalytic efficiency of mixed-phase TiO₂ compared to its single phases [46–48]. At the same time, unambiguous information on the optimal phase composition of TiO2, which ensures its highest photocatalytic activity, is not available in the literature; this problem remains under discussion in literature [44,49,50]. For example, the authors of [50] observed a TiO_2 anatase/rutile phase ratio (40%/60%) similar to TiO₂600 in this work with as well maximum photocatalytic activity.

As can be seen from Table 2, samples TiO_2500 and TiO_2600 are characterized by similar values of S_{BET} and pores size. However, TiO_2600 has a higher crystallite size which is a factor that positively effects photocatalytic activity, since, with increasing crystallite sizes, the rate of annihilation of electron–hole pairs decreases [51]. The TiO_2700 sample is characterized by the largest crystallite sizes; however, it has S_{BET} that is almost two times smaller.

Photocatalyst	RhBconc (Volume)	Degradation, %	Photocatalyst Concentration, g/L	Degradation Time, min	Light Source (Power)	Ref.
Commercial Degussa P25 TiO ₂ (85% of anatase and 15% of rutile)	10 mg/L (40 mL)	95	2.5	150	GYZ220 high-pressure xenon lamp (150 W)	[32]
TiO ₂ (anatase) synthesized by a hydrothermal process	20 mg/L (1000 mL)	80	0.5	180	HL100CH-5 lamp (intensity of 6.5 mW/cm ²)	[33]
Nano-TiO ₂ (pure anatase) microwave hydrothermal method	10 mg/L (60 mL)	84	25	60	high pressure mercury lamp (500 W)	[34]
Flower-like TiO ₂ (rutile) synthesized by a one-step hydrothermal route	10 mg/L (50 mL)	~45	1.0	50	100 W mercury lamp	[35]
Commercial nano anatase ${ m TiO}_2$	30 mg/L (50 mL)	100	2.0	30	A 400 W ultraviolet metal halogen lamp	[36]
TiO ₂ nanostructures (anatase)	6 mg/L (100 mL)	95	2.5	195	UV lamp E_{photon} (eV) 4.43–12.4 with λ_{max} (nm) 280–100	[37]
TiO ₂ fibers (40% of anatase phase and 60% of rutile)	12 mg/L (500 mL)	100	0.6	20	Mercury lamp high-pressure (250 W, 365 nm)	This work

Table 4. Comparison of the photocatalytic activity of TiO₂.

In order to obtain new catalytic materials, it is important to compare their effectiveness with existing analogues. Unfortunately, a direct comparison of the effectiveness of the catalysts is extremely difficult due to the different power of the lamps used in the experiments, different weight of the catalyst, the initial concentration of the dye, etc. However, it is possible to draw indirect conclusions. The data presented in Table 4 show the high activity of the photocatalyst formed in this work, if we take time and completeness of dye degradation as a basis for comparison. To explain the high activity, in addition to its biomorphic hierarchical structure and the characteristics of the phase composition of

Catalysts 2020, 10, 541 9 of 14

the fibers, the shape of the particles of the photocatalyst can play an important role, e.g., see in Table 4. There are no fiber-like particles, while there is an opinion that particles with an elongated shape can exist. This can act as microantennas, adsorbing light quanta more efficiently than particles of a spherical or other shape [52]. Therefore, the fiber-like particles can have higher photocatalytic properties.

3. Materials and Methods

3.1. Fibrous TiO₂ Preparation

To obtain fibrous TiO_2 , a short flaxen fiber was used as a biotemplate (fiber length 4–120 mm, thickness 20–30 µm, ash 1.3–1.5%). The fiber was the waste remaining after machining the linen trust. Precursor solutions were prepared by hydrolysis of titanium chloride ($TiCl_4$) (Sigma-Aldrich Rus, Moscow, Russia) at room temperature in accordance with the procedure described in [22]. For this purpose, initially, $TiCl_4$ was added dropwise to a 6 M HCl solution in order to obtain a solution with a concentration of Ti^{4+} 4.92 M (the concentration of solutions 4.92 M was the limit of ash formation). The obtained highly concentrated solution was slowly diluted with distilled water while continuous stirring until a solution with a residual concentration of Ti^{4+} 0.56 M was obtained (we successfully used it in [25] to get photocatalytic materials by activating hydrothermally the intercalation of titanium polycations). Before using, the precursor solution was aged for 3 h at 20 °C, resulting in the formation of titanium polyhydroxocomplexes.

The biotemplate samples were impregnated with a precursor solution in an autoclave for 5 h at a temperature of 115 °C and a pressure of 170 kPa using a pressure reactor with a fluoroplastic beaker. After treatment, the autoclave was inertially cooled to a room temperature. It should be noted that the choice of moderate parameters (temperature and time) of hydrothermal treatment was due to the prevention of a significant decrease in the specific surface area of the samples because of the formation of large crystallites by using a higher temperature and a long processing time. When the impregnation time was over, the samples were removed from the precursor solution, centrifuged at a peripheral speed of 1500 m/min, and then dried in a desiccator at 95 °C to achieve constant weight. TiO_2 fibrous materials were prepared by calcining impregnated samples of the templates at temperatures of 500, 600, and 700 °C in an electric furnace in air with a constant exposure time of 30 min. Furthermore, these materials were referred to as TiO_2500 , TiO_2600 , and TiO_2700 , where 500, 600, and 700 °C are the calcination temperatures of the templates.

3.2. The Dye under Study

Rhodamine B (RhB, $C_{28}H_{31}ClN_2O_3$, M = 479.02 g/mol), which belongs to the fluorescent dye group [53], was chosen as a model dye (Figure 9). Rhodamine B is highly soluble in water and has high stability to light.

Figure 9. The chemical formula of Rhodamine B.

3.3. The Study of Precursor Solution, Structure, and Properties of Fibrous TiO₂ Samples

The sizes of titanium hydroxocomplexes in the precursor solution were studied by dynamic light scattering on a Zetasizer Nano-ZS analyzer (Malvern Panalytical Ltd., Malvern, UK) at a temperature of 25 $^{\circ}$ C.

Catalysts 2020, 10, 541 10 of 14

The thermal transformations of the biotemplate impregnated with a solution of titanium hydroxocomplexes were studied on a STA 449 F3 Jupiter (Netzsch, Selb, Germany) synchronous thermal analysis device under air atmosphere with a heating rate of 5 °C/min. The flaxen template IR spectra were measured at room temperature on an Avatar 360 ESP Fourier transform spectrophotometer in the wavelength range of $400-4000~\rm cm^{-1}$ with a resolution of 2 cm⁻¹ and averaging of 64 scans. The surface morphology of TiO_2 samples was studied using a Zeiss MERLIN scanning electron microscope (ZEISS, Oberkochen, Germany). X-ray phase analysis was performed on a Bruker D8 Advance X-ray diffractometer (Bruker-AXS, Karlsruhe, Germany). The average crystallite size (L) of TiO_2 phases—anatase and rutile—was evaluated by the Scherrer method [54]:

$$L = \frac{k\lambda}{\beta\cos\theta},\tag{3}$$

where k is the dimensionless particle shape coefficient (0.94), λ is the x-ray wavelength (λ = 0.15425 nm), β is the width of the reflex at half maximum (in units of 2θ), and θ is the diffraction angle. The textural characteristics and the average pore diameter of the samples were determined by the method of low-temperature nitrogen adsorption-desorption on a specific surface and porosity analyzer NOVAtouch LX (Quantachrome Instruments, Boynton Beach, FL, USA); the samples were degassed prior to measurements at 180 °C for three hours.

3.4. Evaluation of the Photocatalytic Activity

The photocatalytic activity of the obtained samples of fibrous TiO₂ was evaluated by studying the rate of destruction of RhB in an aqueous solution under the influence of UV radiation. The source of UV radiation was a high-pressure mercury lamp with a power of 250 W (Philips, Amsterdam, The Netherlands) with a maximum radiation at 365 nm. The lamp, located in a water-cooled quartz jacket, was placed in the center of the reaction vessel with a volume of 800 mL. At the bottom of the reactor, there was a magnetic stirrer, which provided effective mixing of the reaction mass. The reaction solution was purged with air at a constant rate to ensure a constant concentration of dissolved oxygen in it. In each experiment, a weighed portion of the obtained photocatalyst powder in an amount of 0.3 g (0.6 g/L) was added to a RhB dye solution (500 mL) with a concentration of 12 mg/L. The reaction mixture was stirred for a predetermined time (up to 120 min) at a temperature of 25 °C. At certain time intervals, 3 mL of the suspension were selected. Next, the dye solution was separated from the photocatalysts by centrifugation at 8000 rpm for 15 min. The dye concentration in the solutions before and after treatment in a photocatalytic reactor was determined photometrically using a Hitachi U2001 UV VIS, (Mettler Toledo, Columbus, OH, USA) spectrophotometer (wavelength range 200–800 nm), by measuring the optical density at a wavelength corresponding to the maximum absorption spectrum for RhB (λ_{max} = 554 nm). Preliminary irradiation of dye solutions for 1 h in the absence of photocatalysts showed that no significant changes in their optical density occurred during this time. To exclude the influence of sorption processes on dye removal, the reaction systems were pre-saturated for 30 min [25] until adsorption equilibrium was reached without using UV radiation and purging the reaction solution with air. The amount of the adsorbed dye $(q_t, mg/g)$ on the sample over time t was calculated by the equation:

$$q_t = \frac{C_0 - C_t}{m} V,\tag{4}$$

where C_0 and C_t (mg/L) are the initial dye concentration and dye concentration at time t (min), V is the volume of the dye solution (4), m is the weight of the sample of air-dry adsorbent (g). All photocatalytic experiments were repeated twice.

4. Conclusions

The results of this work demonstrate the fundamental possibility of obtaining biomorphic titanium oxide with a hierarchical structure by applying biomimetic solution technology using short

Catalysts 2020, 10, 541 11 of 14

flax fiber as a template. The application of solutions of titanium hydroxocomplexes provides high quality impregnation of the template under hydrothermal conditions, which promotes the nucleation of polymorphic TiO_2 phases and thermal degradation of the impregnated biotemplate during its subsequent annealing in the temperature range of $500\text{--}700\,^{\circ}\text{C}$. All obtained templates of TiO_2 fibers are a mixture of anatase and rutile. Their nanocrystallite sizes are in the range of $16\text{--}45\,\text{nm}$. The $\text{TiO}_2600\,$ sample characterized by the anatase and rutile phase ratio of $40\text{:}60\,$ and the crystallite sizes of about 22 and 28 nm, respectively, demonstrates the highest photocatalytic activity. The Rodamine B dye completely decomposes under UV-irradiation in 20 min using this catalyst. The hierarchical structural organization of biomorfic TiO_2 obtained by solution technology provides this photocatalyst with an advantage compared to other well-known analogs obtained mainly using sol-gel technology.

Author Contributions: Conceptualization, M.F.B., N.E.K., and N.L.O.; methodology, N.E.K., N.L.O., and N.V.Z.; software, N.E.K., N.L.O., D.N.S., and N.V.Z.; validation, M.F.B., N.E.K., and M.M.; formal analysis, M.F.B., N.E.K., N.L.O., and N.V.Z.; investigation, N.E.K., N.L.O., and N.V.Z.; resources, N.E.K. and M.F.B.; data curation, N.E.K., N.L.O., and N.V.Z.; writing—original draft preparation, N.E.K. and N.L.O.; writing—review and editing, M.F.B., N.E.K., D.N.S., and M.M.; visualization, N.E.K., N.L.O., and D.N.S.; supervision, M.F.B. and M.M.; project administration, M.F.B.; funding acquisition, M.F.B. and M.M. All authors have read and agreed to the published version of the manuscript.

Funding: This work was funded by the Ministry of Science and Higher Education of the Russian Federation (Project No. FZZW-2020-0010 and No. 01201260483).

Acknowledgments: The authors would like to thank the ISUCT and Upper Volga Region Centers of Physicochemical Research. Daniel Grüner's and Egbert Wessel's (Forschungszentrum Jülich GmbH) contribution for providing the backscattered images is also appreciated. The authors would like to thank the central library of the Forschungszentrum Jülich GmbH for supporting the publication of this paper with open access.

Conflicts of Interest: The authors declare no conflict of interest.

References

- 1. Maeda, K. Photocatalytic properties of rutile TiO₂ powder for overall water splitting. *Catal. Sci. Technol.* **2014**, *4*, 1949–1953. [CrossRef]
- 2. Chen, J.R.; Qiu, F.X.; Xu, W.Z.; Cao, S.S.; Zhu, H.J. Recent progress in enhancing photocatalytic efficiency of TiO₂-based materials. *Appl. Catal. A Gen.* **2015**, *495*, 131–140. [CrossRef]
- 3. Liu, H.Y.; Joo, J.B.; Dahl, M.; Fu, L.S.; Zeng, Z.Z.; Yin, Y.D. Crystallinity control of TiO₂ hollow shells through resin-protected calcination for enhanced photocatalytic activity. *Energ. Environ. Sci.* **2015**, *8*, 286–296. [CrossRef]
- Buonsanti, R.; Grillo, V.; Giannini, C.; Kipp, T.; Cingolani, R.; Cozzoli, P.D. Nonhydrolytic Synthesis of High-Quality Anisotropically Shaped Brookite TiO₂ Nanocrystals. J. Am. Chem. Soc. 2008, 130, 11223–11233. [CrossRef] [PubMed]
- 5. Bao, S.J.; Bao, Q.L.; Li, C.M.; Dong, Z.L. Novel porous anatase TiO₂ nanorods and their high lithium electroactivity. *Electrochem. Commun.* **2007**, *9*, 1233–1238. [CrossRef]
- Kumar, S.; Lodhi, D.K.; Singh, J.P. Highly sensitive multifunctional recyclable Ag–TiO₂ nanorods SERS substrates for photocatalytic degradation and detection of dye molecules. RSC Adv. 2016, 6, 45120–45126. [CrossRef]
- 7. Zhou, H.; Fan, T.; Zhang, D. Biotemplated Materials for Sustainable Energy and Environment: Current Status and Challenges. *ChemSusChem* **2011**, *4*, 1344–1387. [CrossRef]
- 8. Bian, Z.; Zhu, J.; Li, H.J. Solvothermal alcoholysis synthesis of hierarchical TiO₂ with enhanced activity in environmental and energy photocatalysis. *J. Photochem. Photobiol. C Photochem. Rev.* **2016**, *28*, 72–86. [CrossRef]
- 9. Tang, Y.; Yang, M.; Gao, H.; Li, J.; Wang, G. A facile approach for fabrication of TiO₂ hierarchical nanostructures and their photocatalytic properties. *Colloids Surf. A Physicochem. Eng. Aspects* **2016**, *508*, 184–191. [CrossRef]
- 10. Liu, X.; Zhu, S.; Jiang, H.; Zhou, G.; Chen, Z.; Zhang, D. Sonochemical replication of chloroplast with titania for light harvesting. *Ultrason. Sonochem.* **2011**, *18*, 1043–1047. [CrossRef]
- 11. Hou, H.; Shang, M.; Wang, L.; Li, W.; Tang, B.; Yang, W. Efficient Photocatalytic Activities of TiO₂ Hollow Fibers with Mixed Phases and Mesoporous Walls. *Sci. Rep.* **2015**, *5*, 15228. [CrossRef] [PubMed]

Catalysts 2020, 10, 541 12 of 14

12. Cao, J.; Rusina, O.; Sieber, H. Processing of porous TiO₂-ceramics from biological preforms. *Ceram. Int.* **2004**, *30*, 1971–1974. [CrossRef]

- López Guerrero, M.M.; Vereda Alonso, E.; Garcíade Torres, A.; López Claros, M.; Cano Pavón, J.M. Multivariate optimization of the synthesis of titania biomorphic ceramics and development of a FT-IR method for quantification synthesis yield. *Ceram. Int.* 2013, 39, 7861–7867. [CrossRef]
- 14. Ota, T.; Imaeda, M.; Takase, H.; Kobayashi, M.; Kinoshita, N.; Hirashita, T.; Miyazaki, H.; Hikichi, Y. Porous Titania Ceramic Prepared by Mimicking Silicified Wood. *J. Am. Ceram. Soc.* **2000**, *83*, 1521–1523. [CrossRef]
- 15. Wang, B.; Cheng, J.; Wu, Y. Titania nanotube synthesized by a facile, scalable and cheap hydrolysis method for reversible lithium-ion batteries. Fabrication, characterization and photocatalytic properties of millimeter-long TiO₂ fiber with nanostructures using cellulose fiber as a template. *J. Alloys Compd.* 2012, 527, 132–136. [CrossRef]
- 16. Zhao, J.; Gu, Y.; Huang, J. Flame synthesis of hierarchical nanotubular rutile titania derived from natural cellulose substance. *Chem. Commun.* **2011**, *47*, 10551–10553. [CrossRef]
- 17. Lu, Y.; Sun, Q.; Liu, T.; Yang, D.; Liu, Y.; Li, J. Fabrication, characterization and photocatalytic properties of millimeter-long TiO₂ fiber with nanostructures using cellulose fiber as a template. *J. Alloys Compd.* **2013**, 577, 569–574. [CrossRef]
- 18. Silvestri, S.; Szpoganicz, B.; Hotza, D.; Labrincha, J.A. Synthesis of biomorphic paper-derived anatase. *Mater. Lett.* **2015**, *141*, 275–279. [CrossRef]
- 19. Huang, J.; Kunitake, T. Nano-Precision. Replication of Natural Cellulosic Substances by Metal Oxides. *J. Am. Chem. Soc.* **2003**, *125*, 11834–11835. [CrossRef]
- 20. Esteban Benito, E.; Del Ángel Sánchez, T.; García Alamilla, R.; Hernández Enríquez, J.M.; Sandoval Robles, G.; Paraguay Delgado, F. Synthesis and physicochemical characterization of titanium oxide and sulfated titanium oxide obtained by thermal hydrolysis of titanium tetrachloride. *Braz. J. Chem. Eng.* **2014**, *31*, 737–745. [CrossRef]
- Kochkina, N.E.; Agafonov, A.V.; Vinogradov, A.V.; Karasev, N.S.; Ovchinnikov, N.L.; Butman, M.F. Photocatalytic Activity of Biomorphic TiO₂ Fibers Obtained by Ultrasound-Assisted Impregnation of Cellulose with Titanium Polyhydroxocomplexes. ACS Sustain. Chem. Eng. 2017, 5, 5148–5155. [CrossRef]
- 22. Sterte, J. Synthesis and Properties of Titanium Oxide Cross-Linked Montmorillonite. *Clays Clay Miner.* 1986, 34, 658–664. [CrossRef]
- 23. Vicente, M.A.; Bañares-Muñoz, M.A.; Gandia, L.; Gil, M.A. On the structural changes of a saponite intercalated with various polycations upon thermal treatments. *Appl. Catal. A* **2001**, 217, 191–204. [CrossRef]
- 24. Yuan, P.; Yin, X.; He, H.; Yang, D.; Wang, L.; Zhu, J. Investigation on the delaminated-pillared structure of TiO₂-PILC synthesized by TiCl₄ hydrolysis method. *Microporous Mesoporous Mater.* **2006**, *93*, 240–247. [CrossRef]
- 25. Butman, M.F.; Ovchinnikov, N.L.; Karasev, N.S.; Kochkina, N.E.; Agafonov, A.V.; Vinogradov, A.V. Photocatalytic and adsorption properties of TiO₂-pillared montmorillonite obtained by hydrothermally activated intercalation of titanium polyhydroxo complexes. *Beilstein J. Nanotechnol.* **2018**, *9*, 364–378. [CrossRef]
- 26. Zhang, H.; Ming, R.; Yang, G.; Li, Y.; Li, Q.; Shao, H. Influence of alkali treatment on flax fiber for use as reinforcements in polylactide stereocomplex composites. *Polym. Eng. Sci.* **2015**, *55*, 2553–2558. [CrossRef]
- 27. Titok, V.; Leontiev, V.; Yurenkova, S.; Nikitinskaya, T.; Barannikova, T.; Khotyleva, L. Infrared Spectroscopy of Fiber Flax. *J. Nat. Fibers* **2010**, *7*, 61–69. [CrossRef]
- 28. Castellano, N.; Stipkala, J.M.L.; Friedman, A.; Meyer, G.L. Spectroscopic and excited-state properties of titanium dioxide gels. *Chem. Mater.* **1994**, *6*, 2123–2129. [CrossRef]
- Vasconcelos, D.C.L.; Costa, V.C.; Nunes, E.H.M.; Sabioni, A.C.S.; Gasparon, M.; Vasconcelos, W.L.; Vasconcelos, W.L. Infrared Spectroscopy of Titania Sol-Gel Coatings on 316L Stainless Steel. *Mater. Sci. Appl.* 2011, 2, 1375–1382. [CrossRef]
- 30. Sing, K.S.W.; Everett, D.H.; Haul, R.A.W.; Moscou, L.; Pierotti, R.A.; Rouquérol, J.; Siemieniewska, T. Physical and biophysical chemistry division commission on colloid and surface chemistry including catalysis. *Pure Appl. Chem.* **1985**, *57*, 603–619. [CrossRef]
- 31. De Prez, J.; Van Vuure, A.W.; Ivens, J.; Aerts, G.; Van de Voorde, I. Enzymatic treatment of flax for use in composites. *Biotechnol. Rep.* **2018**, 20, e00294. [CrossRef]

Catalysts 2020, 10, 541 13 of 14

32. Qin, X.; Jing, L.; Tian, G.; Qu, Y.; Feng, Y. Enhanced photocatalytic activity for degrading Rhodamine B solution of commercial Degussa P25 TiO₂ and its mechanisms. *J. Hazard. Mater.* **2009**, 172, 1168–1174. [CrossRef] [PubMed]

- 33. Hieu, N.C.; Lien, T.M.; Van Tran, T.T.; Juang, R.-S. Enhanced removal of various dyes from aqueous solutions by UV and simulated solar photocatalysis over TiO₂/ZnO/rGO composites. *Sep. Purif. Technol.* **2020**, 232, 115962. [CrossRef]
- 34. Chu, Z.; Qiu, L.; Chen, Y.; Zhuang, Z.; Du, P.; Xiong, J. TiO₂-loaded carbon fiber: Microwave hydrothermal synthesis and photocatalytic activity under UV light irradiation. *J. Phys. Chem. Solids* **2020**, *136*, 109138. [CrossRef]
- 35. Wang, Y.; Mo, Z.; Zhang, P.; Zhang, C.; Han, L.; Guo, R.; Gou, H.; Wei, X.; Hu, R. Synthesis of flower-like TiO₂ microsphere/graphene composite for removal of organic dye from water. *Mater. Des.* **2016**, *99*, 378–388. [CrossRef]
- 36. Wang, Z.; Feng, P.; Chen, H.; Yu, Q. Photocatalytic performance and dispersion stability of nanodispersed TiO₂ hydrosol in electrolyte solutions with different cations. *J. Environ. Sci. (China)* **2020**, 32, 59–71. [CrossRef]
- 37. Kiwaan, H.A.; Atwee, T.M.; Azab, E.A.; El-Bindary, A.A. Photocatalytic degradation of organic dyes in the presence of nanostructured titanium dioxide. *J. Mol. Struct.* **2020**, 1200, 127115. [CrossRef]
- 38. Chalastara, K.; Guo, F.; Elouatik, S.; Demopoulos, G.P. Tunable Composition Aqueous-Synthesized Mixed-Phase TiO₂ Nanocrystals for Photo-Assisted Water Decontamination: Comparison of Anatase, Brookite and Rutile Photocatalysts. *Catalysts* **2020**, *10*, 407. [CrossRef]
- 39. Lagergren, S.K. About the Theory of So-Called Adsorption of Soluble Substances. *Kungliga Svenska Vetenskapsakademiens Handlingar Band.* **1898**, 24, 1–39.
- 40. Ho, Y.S.; Mckay, G. The kinetics of sorption of basic dyes from aqueous solution by sphagnum moss peat. *Can. J. Chem. Eng.* **1998**, *76*, 822–827. [CrossRef]
- 41. Gupta, S.S.; Bhattacharyya, K.G. Kinetics of adsorption of metal ions on inorganic materials: A review. *Adv. Colloid Interface Sci.* **2011**, 162, 39–58. [CrossRef] [PubMed]
- 42. Gerasimova, T.V.; Evdokimova (Galkina), O.L.; Kraev, A.S.; Ivanov, V.K.; Agafonov, A.V. Micro-mesoporous anatase TiO₂ nanorods with high specific surface area possessing enhanced adsorption ability and photocatalytic activity. *Microporous Mesoporous Mater.* **2016**, 235, 185–194. [CrossRef]
- 43. Likodimos, V.; Chrysi, A.; Calamiotou, M.; Fernández-Rodríguez, C.; Doña-Rodríguez, J.; Dionysiou, D.; Falaras, P. Microstructure and charge trapping assessment in highly reactive mixed phase TiO 2 photocatalysts. *Appl. Catal. B Environ.* **2016**, *192*, 242–252. [CrossRef]
- 44. Luo, Z.; Poyraz, A.S.; Kuo, C.H.; Miao, R.; Meng, Y.T.; Chen, S.Y.; Jiang, T.; Wenos, C.; Suib, S.L. Crystalline Mixed Phase (Anatase/Rutile) Mesoporous Titanium Dioxides for Visible Light Photocatalytic Activity. *Chem. Mater.* **2015**, 27, 6–17. [CrossRef]
- 45. El-Sheikh, S.M.; Khedr, T.M.; Zhang, G.; Vogiazi, V.; Ismail, A.A.; O'Shea, K.; Dionysiou, D.D. Tailored synthesis of anatase–brookite heterojunction photocatalysts for degradation of cylindrospermopsin under UV–Vis light. *Chem. Eng. J.* 2017, 310, 428–436. [CrossRef]
- 46. Gai, L.; Duan, X.; Jiang, H.; Mei, Q.; Zhou, G.; Tian, Y.; Liu, H. One-pot synthesis of nitrogen-doped TiO₂ nanorods with anatase/brookite structures and enhanced photocatalytic activity. *CrystEngComm* **2012**, *14*, 7662–7671. [CrossRef]
- 47. Boehme, M.; Ensinger, W. Mixed Phase Anatase/rutile Titanium Dioxide Nanotubes for Enhanced Photocatalytic Degradation of Methylene-blue. *Nano Micro Lett.* **2011**, *3*, 236–241. [CrossRef]
- Tay, Q.L.; Liu, X.F.; Tang, Y.X.; Jiang, Z.L.; Sum, T.C.; Chen, Z. Enhanced Photocatalytic Hydrogen Production with Synergistic Two-Phase Anatase/Brookite TiO₂ Nanostructures. J. Phys. Chem. C 2013, 117, 14973–14982.
 [CrossRef]
- 49. Kääriäinen, M.-L.; Kääriäinen, T.O.; Cameron, D.C. Titanium dioxide thin films, their structure and its effect on their photoactivity and photocatalytic properties. *Thin Solid Films* **2009**, *517*, 6666–6670. [CrossRef]
- 50. Allen, N.S.; Mahdjoub, N.; Vishnyakov, V.; Kelly, P.J.; Kriek, R.J. The effect of crystalline phase (anatase, brookite and rutile) and size on the photocatalytic activity of calcined polymorphic titanium dioxide (TiO₂). *Polym. Degrad. Stab.* **2018**, *150*, 31–36. [CrossRef]
- 51. Son, H.-J.; Wang, X.; Prasittichai, C.; Jeong, N.C.; Aaltonen, T.; Gordon, R.G.; Hupp, J.T. Glass-Encapsulated Light Harvesters: More Efficient Dye-Sensitized Solar Cells by Deposition of Self-Aligned, Conformal, and Self-Limited Silica Layers. *J. Am. Chem. Soc.* 2012, 134, 9537–9540. [CrossRef] [PubMed]

Catalysts 2020, 10, 541 14 of 14

52. Agafonov, A.V.; Afanasyev, D.A.; Gerasimova, T.V.; Krayev, A.S.; Kashirin, M.A.; Vinogradov, V.V.; Vinogradov, A.V.; Kessler, V.G. Nanoparticle Self-Assembly Mechanisms in the Colloidal Synthesis of Iron Titanate Nanocomposite Photocatalysts for Environmental Applications. *ACS Sustain. Chem. Eng.* **2016**, *4*, 2814–2821. [CrossRef]

- 53. Gordon, P.F.; Gregory, P. Organic Chemistry in Colour; Springer-Verlag: Berlin, Germany, 2012. [CrossRef]
- 54. Langford, J.I.; Wilson, A.J.C. Scherrer after sixty years: A survey and some new results in the determination of crystallite size. *J. Appl. Cryst.* **1978**, *11*, 102–113. [CrossRef]



© 2020 by the authors. Licensee MDPI, Basel, Switzerland. This article is an open access article distributed under the terms and conditions of the Creative Commons Attribution (CC BY) license (http://creativecommons.org/licenses/by/4.0/).